Proceedings of the ASME 2022
International Mechanical Engineering Congress and Exposition
IMECE2022
October 30-November 3, 2022, Columbus, Ohio

IMECE2022-93929

PROTOTYPE DESIGN AND MANUFACTURE OF A DEPLOYABLE TENSEGRITY MICROROBOT

Christian Kazoleas[1]
A. Leon Linton Department of Mechanical, Robotics and Industrial Engineering, Lawrence Technological University
Southfield, MI, 48075

Kaushik Mehta[1]
A. Leon Linton Department of Mechanical, Robotics and Industrial Engineering, Lawrence Technological University
Southfield, MI, 48075

Sichen Yuan[2]
A. Leon Linton Department of Mechanical, Robotics and Industrial Engineering, Lawrence Technological University
Southfield, MI, 48075

ABSTRACT

Micro-, and milli-scale robots have been of great R&D interest, due to their ability to accomplish difficult tasks such as minimally invasive diagnosis and treatment for human bodies, and underground or deep-sea tests for environment monitoring. A good solution to this design need is a multi-unit deployable tensegrity microrobot. The microrobot can be folded to only 15% of its deployed length, so as to easily enter a desired working area with a small entrance. When deployed, the tensegrity body of the robot displays lightweight and high stiffness to sustain loads and prevent damage when burrowing through tightly packed tissues or high-pressure environments. In this work, topology, initial configuration and locomotion of a deployable tensegrity microrobot are determined optimally. Based on the design, a centimeter-scale prototype is manufactured by using a fused deposition modelling advanced additive manufacturing or 3-D printing system for proof of concept. As shown in experimental results, the deployable tensegrity microrobot prototype designed and manufactured can achieve an extremely high folding ratio, while be lightweight and rigid. The locomotion design, that mimics a crawling motion of an earthworm, is proved to be efficient by the prototype equipped with stepper motors, actuation cables, control boards and a braking system.

Keywords: microrobot; additive manufacturing; tensegrity structure; deployable structure; bio-mimic locomotion; magnetic actuation

NOMENCLATURE

T	member internal force
r	unit vector of member direction
L	member length
M	equilibrium matrix
p	vector of external force
n	number of nodes
k	number of members
c	number of constraints
m	number of mechanisms
s	state of self-stress

1. INTRODUCTION

The concept of tensegrity structure was first introduced in the 1940s, when it was only used in architecture design, based on the concept of the human anatomy of bones held by tendons [1]. Tensegrity comes from two words, tensional integrity, which represents a structure that is in tension and still rigid [2]. A tensegrity structure can maintain its desired shape without complex joints or mechanisms, which are commonly seen in umbrella- or origami-shape deployable structures [3, 4]. A tensegrity structure is composed of a network of cables in tension and several non-touch bar members under continuous compression. Such assembly produces a lightweight, deployable, and yet self-standing structure with high stiffness [5].

Recently, tensegrity structures have been successfully applied in design of robots. The first design was carried out by Shibata et al. [6], in which a crawling robot was built by a single tensegrity unit. This concept was later used in design of the

[1] Undergraduate student.
[2] Assistant professor, corresponding author. email: syuan@ltu.edu

Spherical Underactuated Planetary Exploration Robot (SUPER-ball) [7, 8], which is a compliant icosahedron tensegrity robot for planetary landing and exploration. Mirletz et al. [9] developed a spine-like robot, which aims at an adaptation for traversing multiple terrains, by combing multiple tensegrity units. Other designs, such as DuCTT robot [10, 11] and tensegrity manipulators [12], proved that tensegrity structure is also an effective solution for robot design in accomplishing various types of tasks, such as exploring duct systems and achieving human biomechanical motions.

Micro-, and milli-scale robots have been of great R&D interest, due to its ability to accomplish difficult tasks such as minimally invasive diagnosis and treatment for human bodies, and underground or deep-sea tests for environment monitoring. A good solution to this design need is a multi-unit deployable tensegrity microrobot [13]. The microrobot can be folded to only 15% of its deployed length, so as to easily enter a desired working area with a small entrance. When deployed, the tensegrity body of the robot displays lightweight and high stiffness to sustain loads and prevent damage when burrowing through tightly packed tissues or high-pressure environments. A locomotion of the tensegrity microrobot is designed to mimic a crawling motion of an earthworm, which grants the robot an ability to move well through small working areas.

An essential component in development of such a deployable tensegrity microrobot is its prototype design and manufacture. In this work, topology, initial configuration, and locomotion of the deployable tensegrity microrobot are determined optimally. Based on the design, a centimeter-scale prototype is manufactured by using a fused deposition modeling advanced additive manufacturing or 3-D printing system for proof of concept. The prototype designed and manufactured shall be verified by experiments with respect to its folding ratio and locomotion efficiency.

2. PROTOTYPE DESIGN

Topology design and form finding are two essential components in design of a tensegrity structure. Topology design is to determine numbers of nodes and members, and the corresponding member connectivity. Form finding is determination of geometric configuration and internal force distribution among members of a tensegrity structure. Based on the approaches given in Ref. [13], topology design and form finding of the deployable tensegrity microrobot under investigation are presented in this section.

To mathematically formulate the design problem, the equation of force equilibrium of a tensegrity structure is presented. The force equilibrium equation is determined by structural topology, nodal positions, and member internal forces. This equation serves as a fundamental rule of structural design and analysis (for example, form finding). A general member that connects the *i*-th and *j*-th nodes of a tensegrity structure is shown in Fig. 1. The force equilibrium equation of *i*-th node can be written as

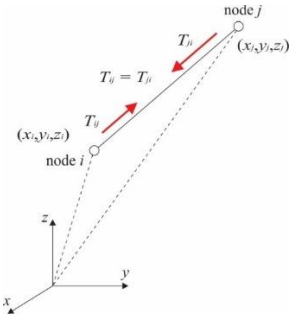

FIGURE 1: A GENERAL MEMBER THAT CONNECTS TWO NODES OF A TENSEGRITY STRUCTURE

$$\sum_j T_{ij} r_{ij} + p_i = 0 \tag{1}$$

In Eq. (1), p_i is the external load applied to the *i*-th node; T_{ij} and r_{ij} are magnitude and unit direction vector of internal force of a member that connects the *i*-th and *j*-th nodes. r_{ij} is determined by nodal coordinates:

$$r_{ij} = \begin{bmatrix} x_j - x_i \\ y_j - y_i \\ z_j - z_i \end{bmatrix} \frac{1}{L_{ij}} \tag{2}$$

L_{ij} is the deformed (tensioned or compressed) length of the member:

$$L_{ij} = \sqrt{(x_j - x_i)^2 + (y_j - y_i)^2 + (z_j - z_i)^2} \tag{3}$$

By substituting Eq. (2) into the force equilibrium equation (1) and taking all free nodes of a tensegrity structure into consideration, the general form of force equilibrium equation is obtained as

$$MT + p = 0 \tag{4}$$

where M is a $3n$ by k equilibrium matrix that contains the direction cosines; T is a k by 1 vector of member internal forces; p is a $3n$ by 1 vector of external forces applied at nodes. n is the number of nodes, and k is the number of members of a tensegrity structure. In the design stage of a tensegrity structure, the external load is usually assumed zero. Then Eq. (4) can be rewritten as

$$MT = 0 \tag{5}$$

2.1 Topology design

A topology design is composed of two tasks: determination of numbers of nodes and members, and generation of member connectivity. A topology design of the deployable tensegrity

microrobot under investigation must follow the extended Maxwell's rule:

$$3n - k - c = m - s \tag{6}$$

where c is the number of nodal-position constraints. m is the number of mechanisms, and s is the state of self-stress, which are calculated from the equilibrium matrix M in Eq. (5)

A topology design of the robot is presented in Fig. 2. The robot is composed of two end units and several intermediate units. To achieve a lightweight, deployable structure while still having a rigid body, a six-bar member tensegrity structure is formed as a unit cell, see Fig. 3. The six bar members are identical, allowing a quick and easy production in fabrication process. Similarly, two bar members are placed in the same plane, separated by half of their total lengths. A cable network is then attached to the bar members, forming eight equilateral triangles on the unit cell. The unit cell is a class-1 tensegrity structure without contacts among bar members. Note that such a class-1 tensegrity is preferred in design of deployable tensegrity microrobot due to the avoidance of including complex mechanisms for bar-to-bar connection, which will likely increase the chance of failure in robot morphing.

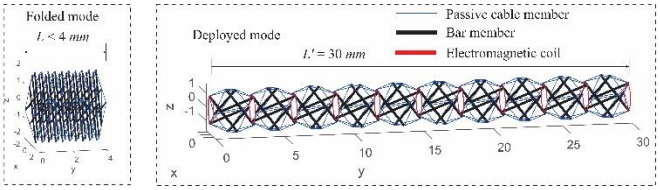

FIGURE 2: A PERSPECTIVE VIEW OF A DEPLOYABLE TENSEGRITY MICROROBOT

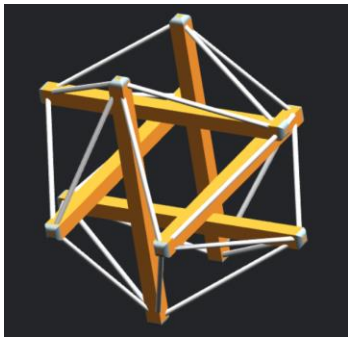

FIGURE 3: TOPOLOGY OF A UNIT CELL OF THE DEPLOYABLE TENSEGRITY MICROROBOT

2.2 Form finding

An initial configuration of the deployed tensegrity microrobot is determined by the stochastic fixed nodal position method (SFNPM) [14, 15]. In this method, nodes of a tensegrity structure can be placed freely at any desired positions; then, a distribution of member internal forces is assigned by a stochastic optimization algorithm. Unlike traditional form-finding methods that usually lack correlation between member internal forces and geometric configuration, the SFNPM employs a form-finding task as a displacement first and stress later procedure, allowing nodes of the structure to be placed freely at any desired position. At the same time, the optimal self-stress determination in the second part of the SFNPM yields good structural stability.

2.3 Bio-mimic locomotion design

Locomotion of the tensegrity microrobot is designed to mimic a crawling motion of an earthworm. It is assumed that a full forward crawling step of the robot starts at its folded mode, see Phase 1 in Fig. 4. During a crawling movement, unit cells of the robot take turns to morph. To move forward, electromagnetic coils in the front of the body generate magnetic forces of repulsion. These forces will increase lengths and decrease diameter of front unit cells, and thereby increasing the pressure of the front end, allowing the robot to reach forward, see Phase 2 in Fig. 4. The robot also relies on anchors, similar to setae of an earthworm, to hold onto the ground surface. When Phase 2 is complete, the anchors extend out of the body and hold the front of its body to the ground surface. Then, current directions of electromagnetic coils in the front of the body are reversed, providing magnetic forces of attraction. Thus, unit cells in the front of the body are contracted, pulling the back of the body forward. To smooth the pulling process, forces of attraction in the back of the body are gradually released. Thus, cells in the back of the body are in their deployed mode when being pulled forward, see Phase 3 in Fig. 4. Finally, all unit cells of the robot are pulled forward, and the robot morphs back to its folded mode. The anchors from the front of the body retract, and the anchor in the back of the body extends out to hold the body on the surface; see Phase 4 in Fig. 4. Phase 1-4 are repeated for another full forward crawling step of the robot.

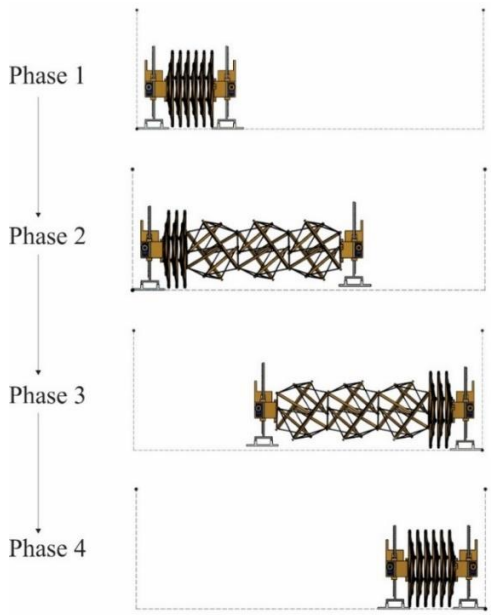

FIGURE 4: FORWARD MOVEMENT OF THE DEPLOYABLE TENSEGRITY MICROROBOT THAT MIMICS A CRAWLING MOTION OF AN EARTHWORM

3. PROTOTYPE MANUFACTURE

The topology design, form finding, and locomotion design introduced in Section 2 need to be verified by experimental results, which call for a feasible approach to prototype manufacture. In this work, a centimeter-scale prototype is manufactured for proof of concept. In the manufacturing process, the issue of losing shape accuracy in traditional tensegrity robot fabrication techniques shall be avoided by using a fused deposition modeling advanced additive manufacturing or 3-D printing system. Thus, a high structure shape accuracy can be achieved. The prototype is composed of six almost identical unit cells, with a braking system, which serve as anchors of the robot introduced in Section 2.3 with two parts being attached at the two ends of the robot. Note that the prototype is much larger in size than that designed in Section 2, in order to facilitate fast assembling and testing. The prototype is motivated by stepper motors placed at centers of the unit cells instead of the electromagnetic coils originally designed.

3.1 Bar and Cable members

Using the Ultimaker-S3, each bar is made out of Tough polylactic acid (PLA), an advanced PLA with increased impact-resistant properties. Two different bars are used for the tensegrity structure: regular and motor bar members. There are five standard bar members in a unit cell. Each bar has a height of 3*mm*, a width of 3*mm*, and a length of 154*mm*. Also, as seen in Fig. 5 (a), the bars have a peg on top, allowing for easy cable member attachment. The bar member shown in Fig. 5 (b) is a motor bar. Only one motor bar member is used in a unit cell. The motor bar member is used to hold a stepper motor in place while the motor shaft rotates during robot morphing.

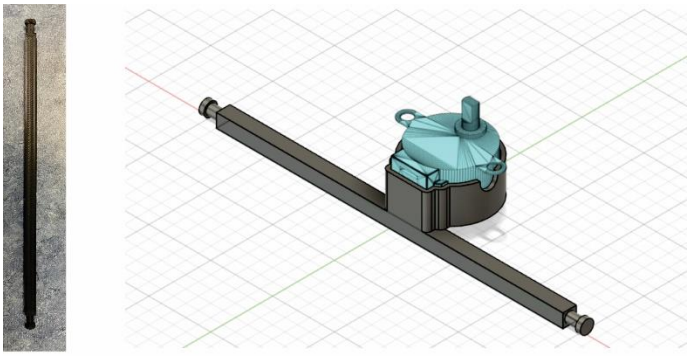

(a) (b)

FIGURE 5: (A) A REGULAR BAR MEMBER; (B) A MOTOR BAR MEMBER

A cable network consisting of eight equilateral triangles, see Fig. 6, is printed by Hyrel system 30M printer with NINJAFLEX being the material. These triangles are designed to have holes at interconnecting points, which allows for a quick attachment to the bar members. Note that the cable triangles are printed separately to ensure high fabrication accuracy, shown in Fig. 7. Although the eight triangles can be fabricated together in a single printing procedure.

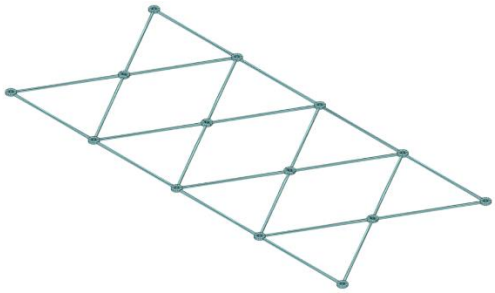

FIGURE 6: CAD MODEL OF THE CABLE NETWORK WITH EIGHT EQUILATERAL TRANGLES.

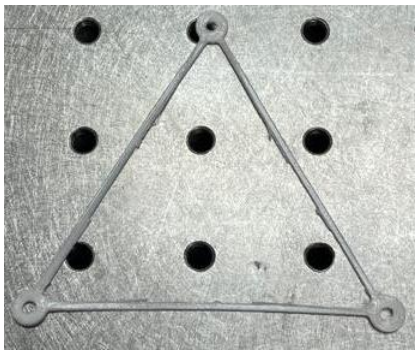

FIGURE 7: AN EQUILATERIAL TRANGLE OF CABLE NETWORK PRINTED BY NINJA-FLEX.

3.2 Braking system

The braking system shall serve as anchors, similar to setae of an earthworm, to hold the ground position at the two ends of the robot while the body is morphing, shown in the locomotion design. A fabricated part of the braking system is given in Fig. 8. The two braking parts operate inversely: for example, when the front part is placed down, the back part is pulled up. The pad is raised when the braking system is active in the up position. Now, most of the ninja NINJAFLEX pad is off the ground. However, a small portion of the front area will be in contact but does not affect the performance since the edge will not have enough weight concentrated on it, hindering the motion.

FIGURE 8: A PART OF THE BRAKING SYSTEM

With the fabricated bar and cable members, and the braking system, a final assembly of the deployable tensegrity microrobot prototype with six unit cells is shown in Fig. 9.

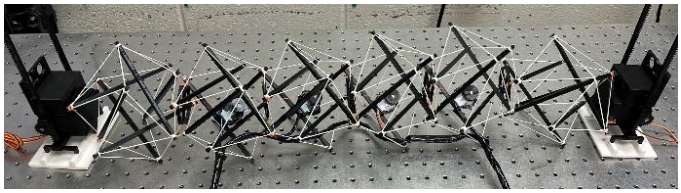

FIGURE 9: A FINAL ASSEMBLY OF THE DEPLOYABLE TENSEGRITY ROBOT PROTOTYPE

3.3 Actuation and control

The morphing mechanism of the deployable tensegrity microrobot prototype is shown in Fig. 10. In the deployable tensegrity microrobot prototype, unipolar stepper motors are used for morphing of the tensegrity robot due to their micro-stepping capabilities and high torques. When a stepper motor in a unit cell spins to reel the actuation cables around the attached pulley, the two sides of the unit cell are pulled together, so as to compress the unit cell in a folded mode. Once in folded mode, the unit cell can deploy by rotating the stepper motor in the reverse direction. A deployed mode will finally be reached by the potential energy stored in cable members.

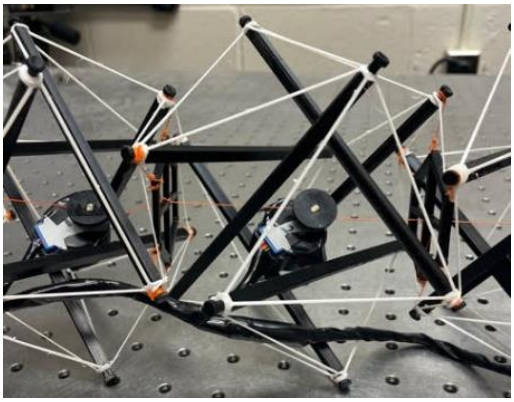

FIGURE 10: MORPHING MECHANISM OF THE DEPLOYABLE TENSEGRITY MICROROBOT PROTOTYPE.

The control system of the tensegrity microrobot prototype is shown in Fig. 11. During morphing of the deployable tensegrity microrobot prototype, the structure must have an onboard control system with multiple boards of size 50*mm* by 50*mm*, connected to a 12*Volt* parallel battery line. Each board controls two stepper motors. Since these boards are separated, a 2.4*GHz* NRF24L01 trans receiver module is added for communication among these boards. The processor used is STM32F103C8T6, which can provide sufficient digital pins to control steppers, servos, ultrasonic sensors, and the NRF24L01 trans receiver. This design will yield a board with an optimized size.

FIGURE 11: A PCB BOARD DESIGN WITH TRANSMITTER

4. EXPERIMENT

Efficiency of the deployable tensegrity microrobot prototype manufactured in Section 3 is validated by two experiments in this section: a folding test and a locomotion test. The folding test is to prove the efficiency of the electromagnetic morphing system to be used by the deployable tensegrity robot in microscale. This means the braking system and the controls are taken off. The locomotion test is used to validate the locomotion design that mimics a crawling motion of an earthworm. This means the stepper motors and the braking system are integrated into the prototype.

4.1 Folding test

Folding tests in this work are completed by the MTS Criterion M41 universal testing system. In these tests, a unit cell of the prototype and a whole prototype structure with six unit cells are placed on the testing system for folding tests, see Fig. 12. During the folding tests, compressive loads are applied to the two structures to mimic the magnetic forces for robot morphing. The load-displacement relationships of these two structures are shown in Figs. 13 and 14, and the testing results are summarized in Table 1. As seen in Table 1, the peak compressive loads to fully compress the unit cell and the whole prototype structure are 4.31*N* and 4.42*N*, respectively, with a difference being only 2.54%. This is within a reasonable range of the magnetic force to be generated by the electromagnetic coils. As seen in Table 2, the folding ratios of the unit cell and the whole prototype structure are 18.00% and 12.47%, respectively, which proves the efficiency of the topology design given in this work.

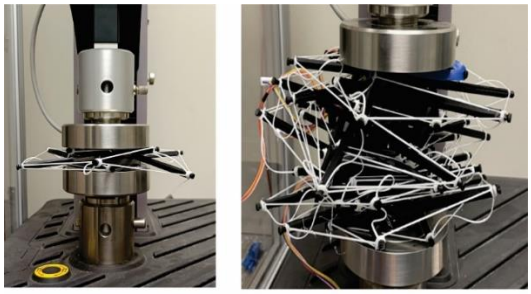

(a) (b)

FIGURE 12: FOLDING TEST ON (A) A SINGLE UNIT CELL; (B) THE WHOLE PROTOTYPE STRUCTURE

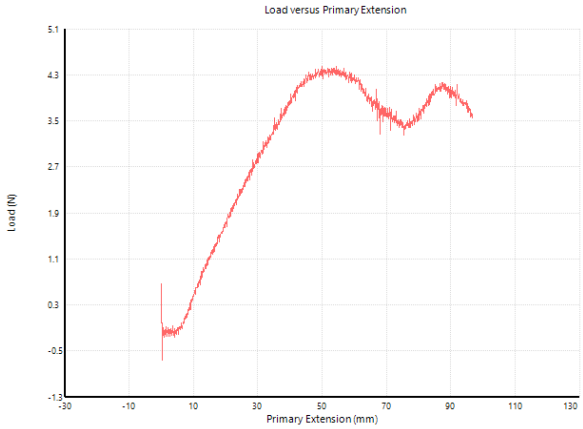

FIGURE 13: FOLDING TEST OF A SINGLE UNIT CELL

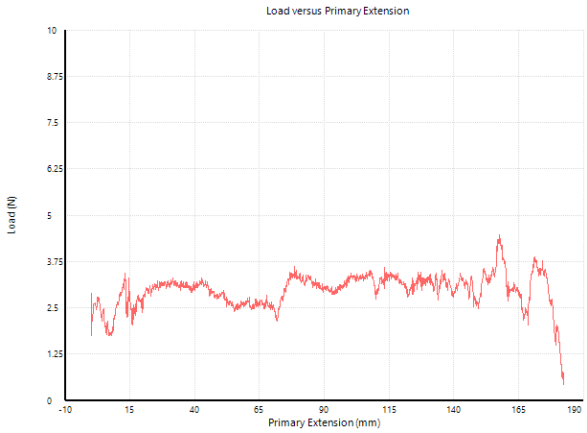

FIGURE 14: FOLDING TEST OF THE WHOLE PROTOTYPE STRUCTURE

TABLE 1: PEAK LOADS OF THE SINGLE UNIT CELL AND THE WHOLE PROTOTYPE STRUCTURE IN FOLDING TESTS

	Peak load (*N*)	Difference
Single unit cell	4.31	2.54%
Whole prototype structure	4.42	

TABLE 2: FOLDING RATIOS OF THE SINGLE UNIT CELL AND THE WHOLE PROTOTYPE STRUCTURE

	Deployed length (*mm*)	Folded length (*mm*)	Folding ratio
Single unit cell	125.1	22.5	18.00%
Whole prototype structure	783.3	97.7	12.47%

4.2 Locomotion test

A locomotion test is performed on the completely assembled prototype, with stepper motors, actuation cables, control boards, and a braking system equipped. A 12*Volt* power supply is applied to the control boards, which run the following sequence: the front braking part is first activated to hold its ground position; then the stepper motors take turns to rotate, thus compressing the prototype to its folding mode; once a complete folding mode is reached, the front braking part is released, and the rear braking part is activated to hold its ground position; finally the stepper motors take turns to rotate in directions opposite to the folding procedure; finally the prototype extends to its deployed mode by the potential energy stored in its cable members.

The deployed length of the prototype is 846.7*mm*, which is longer than that in the folding testing. This is due to the incorporation of the braking system. When the prototype reaches its folding mode, the body length is 450.27*mm*, achieving a folding ratio of 46.82%, shown in Table 3. Note that this folding ratio is significantly lower than that obtained in the folding test. This downgrade in performance is mainly caused by the large sizes of stepper motors placed at centers of unit cells. This issue is expected to be solved by incorporating electromagnetic coils in the prototype to replace the stepper motors.

TABLE 3: FOLDING RATIO COMPARISON OF THE FOLDING TESTS

	Deployed length (*mm*)	Folded length (*mm*)	Folding ratio
Actual case	846.7	450.3	46.82%

A locomotion test is presented in Fig. 15. A magnetic block is placed at the initial starting spot of the prototype as a position reference. When powered, the prototype shows an efficient movement: one full cycle of movement (deployed-folded-deployed) takes only 20 seconds, while moving forward by a distance of 157.88*mm*. This prototype can travel over 1 meter in 6 movement cycles, with an average velocity of 7.894*mm/s*. Similar efficiency can be expected in a micro-scale deployable tensegrity robot prototype powered by electromagnetic coils. The electromagnetic coil, which are to be investigated in future work, will be attached to the inside structure tangent of each inner node. Thus, the actual size of the coil will be determined

based on the diameter of the microrobot. This usage of the electromagnetic coil will allow the robot to reach almost perfect compression; thus, the locomotion efficiency will be significantly improved.

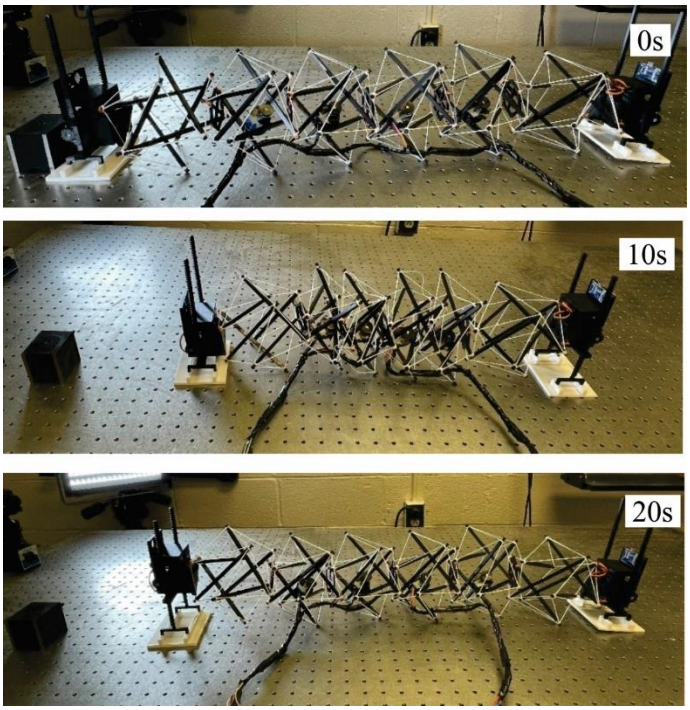

FIGURE 15: LOCOMOTION TEST OF THE DEPLOYABLE TENSEGRITY MICROROBOT PROTOTYPE

5. CONCLUSION

Topology design, form finding, and locomotion design of a deployable tensegrity microrobot are presented in this work. A centimeter-scale prototype for proof of concept is manufactured by using a fused deposition modeling advanced additive manufacturing or 3-D printing system. As shown in experimental results, the manufactured prototype possesses an extremely high folding ratio while being lightweight and rigid. High locomotion efficiency is seen in the prototype when equipped with stepper motors, actuation cables, control boards, and a braking system.

ACKNOWLEDGEMENTS

The authors acknowledge support from the US NSF (National Science Foundation) through grant 2104237.

REFERENCES

[1] Chen, C. S., and Ingber, D. E., 1999, "Tensegrity and mechanoregulation: from skeleton to cytoskeleton," *Osteoarthritis and Cartilage*, 7(1), pp. 81-94.

[2] Pugh, A., 2020, "An introduction to tensegrity," An Introduction to Tensegrity, University of California Press.

[3] Yuan, S., and Jing, W., 2021, "Optimal Shape Adjustment of Large High-Precision Cable Network Structures," *AIAA Journal*, 59(4), pp. 1441-1456.

[4] Miyashita, S., Guitron, S., Ludersdorfer, M., Sung, C. R., and Rus, D., "An untethered miniature origami robot that self-folds, walks, swims, and degrades," *Proc. 2015 IEEE International Conference on Robotics and Automation (ICRA)*, IEEE, pp. 1490-1496.

[5] Snelson, K., 1996, "Snelson on the tensegrity invention," *International Journal of Space Structures*, 11(1-2), pp. 43-48.

[6] Shibata, M., Saijyo, F., and Hirai, S., "Crawling by body deformation of tensegrity structure robots," *Proc. 2009 IEEE international conference on robotics and automation*, IEEE, pp. 4375-4380.

[7] Bruce, J., Caluwaerts, K., Iscen, A., Sabelhaus, A. P., and SunSpiral, V., "Design and evolution of a modular tensegrity robot platform," *Proc. 2014 IEEE International Conference on Robotics and Automation (ICRA)*, IEEE, pp. 3483-3489.

[8] Sabelhaus, A. P., Bruce, J., Caluwaerts, K., Manovi, P., Firoozi, R. F., Dobi, S., Agogino, A. M., and SunSpiral, V., "System design and locomotion of SUPERball, an untethered tensegrity robot," *Proc. 2015 IEEE international conference on robotics and automation (ICRA)*, IEEE, pp. 2867-2873.

[9] Mirletz, B. T., Bhandal, P., Adams, R. D., Agogino, A. K., Quinn, R. D., and SunSpiral, V., 2015, "Goal-directed cpg-based control for tensegrity spines with many degrees of freedom traversing irregular terrain," *Soft Robotics*, 2(4), pp. 165-176.

[10] Friesen, J., Pogue, A., Bewley, T., de Oliveira, M., Skelton, R., and Sunspiral, V., "DuCTT: A tensegrity robot for exploring duct systems," *Proc. 2014 IEEE International Conference on Robotics and Automation (ICRA)*, IEEE, pp. 4222-4228.

[11] Friesen, J. M., Glick, P., Fanton, M., Manovi, P., Xydes, A., Bewley, T., and Sunspiral, V., "The second generation prototype of a duct climbing tensegrity robot, DuCTTv2," *Proc. 2016 IEEE International Conference on Robotics and Automation (ICRA)*, IEEE, pp. 2123-2128.

[12] Lessard, S., Castro, D., Asper, W., Chopra, S. D., Baltaxe-Admony, L. B., Teodorescu, M., SunSpiral, V., and Agogino, A., "A bio-inspired tensegrity manipulator with multi-DOF, structurally compliant joints," *Proc. 2016 IEEE/RSJ International Conference on Intelligent Robots and Systems (IROS)*, IEEE, pp. 5515-5520.

[13] Yuan, S., Jing, W., and Jiang, H., "A Deployable Tensegrity Microrobot for Minimally Invasive Interventions," *Proc. ASME International Mechanical Engineering Congress and Exposition*, American Society of Mechanical Engineers, p. V005T005A061.

[14] Yuan, S., and Yang, B., 2019, "The fixed nodal position method for form finding of high-precision lightweight truss structures," *International journal of Solids and Structures*, 161, pp. 82-95.

[15] Yuan, S., and Zhu, W., 2021, "Optimal self-stress determination of tensegrity structures," *Engineering Structures*, 238, p. 112003.